

Investigating the Molecular Origins of Responsiveness in Functional Silicone Elastomer Networks

Julie A. Crowe-Willoughby,^{†,§} Derrick R. Stevens,[‡] Jan Genzer,^{*,†} and Laura I. Clarke^{*,‡}

[†]Department of Chemical & Biomolecular Engineering, NC State University, Raleigh, North Carolina 27695-7905, and [‡]Department of Physics, NC State University, Raleigh, North Carolina 27695-8202. [§]Present address: MeadWestvaco, Center for Packaging Innovation, 1021 Main Campus Drive, Raleigh, North Carolina 27606

Received February 28, 2010; Revised Manuscript Received April 25, 2010

ABSTRACT: Dielectric, calorimetric, and dynamic mechanical measurements were performed to delineate the types and dynamic rates of molecular scale motion in modified poly(vinylmethyl siloxane) (PVMS) stimuli-responsive networks, where pendent groups of the form $-\text{S}-(\text{CH}_2)_n-\text{OH}$ were chemically attached to the vinyl moiety of PVMS. The glass transition temperature (T_g) for the unsubstituted PVMS network matches that previously reported for linear PVMS indicating that the flexibility of the polymer chains is unaffected by the network cross-linking. In contrast, T_g increases with the introduction of pendent groups of the type $-\text{S}-(\text{CH}_2)_n-\text{CH}_3$ or $-\text{S}-(\text{CH}_2)_n-\text{OH}$, where n is 2, 6, or 11, as the different groups constrain the siloxane backbone to differing degrees. The macroscopic response time and amplitude, as previously measured by dynamic contact angle, are correlated with the observed glass transition temperatures. One conclusion is that the flexibility of the network and the interactions between pendent groups affect responsiveness.

I. Introduction

Responsive materials alter their physical or chemical properties spontaneously when exposed to an external stimulus (e.g., an electromagnetic field, mechanical strain, temperature variation, exposure to a fluid, or change of pH or ionic strength).^{1–4} While the response is primarily due to structural alterations occurring at the microscopic level, i.e., changes in molecular conformation, these microscopic adjustments result in variations in measurable macroscopic characteristics, such as material shape, size, color, or wetting properties. When considering applications of these stimuli-responsive materials, three quantities are important: (1) the magnitude of the response, (2) the speed of the response, and (3) any hysteresis associated with the switching, such as a long reset time after stimulation. Speed of response should be tunable for specific applications. For instance, an ideal material for sensing possesses a large, fast response with little hysteresis. However, all three of these parameters can be interlinked; e.g., alterations to increase the response magnitude could also unintentionally increase response time.

In this work, we explore the relationship between structural parameters, microscopic dynamics, and macroscopic response time for silicone elastomer networks acting as stimuli-responsive surfaces. We employ differential scanning calorimetry (DSC), dynamic mechanical thermal analysis (DMTA), and dielectric relaxation spectroscopy (DRS) to examine thoroughly various molecular motions in responsive surfaces made from modified poly(vinylmethyl siloxane) (PVMS) networks. We then correlate these molecular motions to the measured macroscopic response (as determined by dynamic contact angle (DCA)) as a function of material structure.

In the PVMS network system, the cross-links of the network provide a solid-like nature, despite the low T_g of linear PVMS

(≈ 150 K) which allows for a high degree of flexibility at room temperature.^{5,6} Due to the difference in surface energies between the vinyl and methyl groups, PVMS is moderately amphiphilic. Because the network is flexible, the side-chains can rearrange readily when placed in contact with another medium, thus delivering the component resulting in the lowest interfacial energy (dependent on the surroundings) to the interface. For instance, the hydrophobic methyl groups are exposed to the surface when the material is placed in air. When in contact with a hydrophilic environment, i.e., water, the more hydrophilic vinyl groups migrate to the surface (Figure 1). As the energy difference between the vinyl and methyl moieties is small, we have grafted mercaptoalkanols at the vinyl group via the thiol–ene reaction thereby increasing the contrast between the opposing termini and enhancing the switching property.^{5,6} We previously studied the kinetics of surface rearrangement of the substituted networks (with pendent $-\text{S}-(\text{CH}_2)_n-\text{OH}$ groups) by monitoring wettability changes using both static and dynamic contact angle measurements. In particular, we established that both the rate and magnitude of switching decreased with increasing length of the methylene spacer (n) separating the $-\text{OH}$ terminus from the siloxane network.^{5,6}

The aim of this work is to observe and characterize the molecular-level dynamics in PVMS-based networks and to determine how these molecular motions are altered by (1) the length of the methylene spacer in the mercaptoalkanol pendent group and (2) the end-terminus of the pendent group ($-\text{OH}$ vs $-\text{CH}_3$). We perform new analysis of data on the macroscopic network response and discuss how the dynamics at a molecular level influence the macroscopic properties. In general, the response time of a stimuli-responsive material will depend not only on the magnitude of the interfacial driving force (i.e., the difference in interfacial energy between the two switching states) but also on the innate dynamics within the material. In particular, in the substituted PVMS networks, the pendent groups must move through the network in order to emerge at the surface; thus the

*Corresponding authors: (L.I.C.) laura_clarke@ncsu.edu; (J.G.) jan_genzer@ncsu.edu.

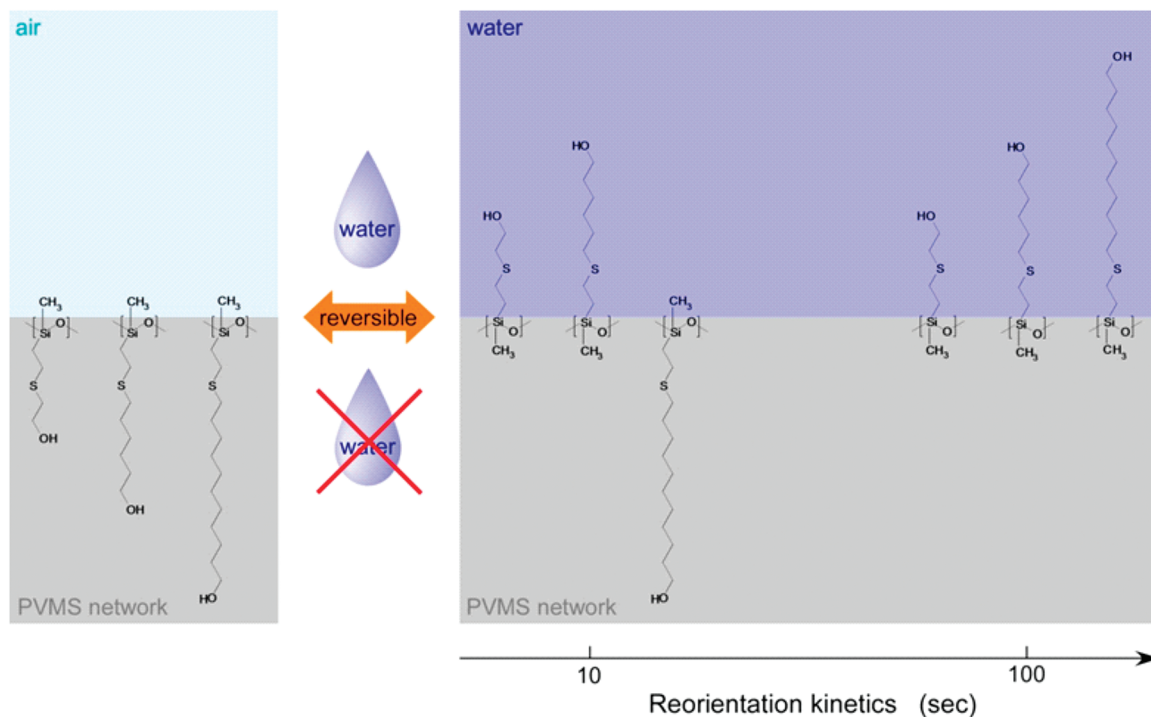


Figure 1. Schematics depicting the reorientation kinetics of PVMS-S-(CH₂)_n-OH samples ($n = 2, 6,$ and 11) between hydrophobic (left) and hydrophilic (right) states.

Table 1. Properties of Bare and Modified Silicone Elastomer Networks Assessed with Differential Scanning Calorimetry (DSC), Dynamical Mechanical Thermal Analysis (DMTA), and Dielectric Relaxation Spectroscopy (DRS)

material	T_g (K) ^a			T_m (K) ^b			Local mode (K)	
	DSC	DMTA ^c	DRS ^d	DSC	DMTA ^c	DRS ^e	DMTA ^c	DRS ^f
PDMS		156 ± 5	146–166	230	224	245–250		
PVMS		149 ± 3	140 ± 5					
PVMS-S-(CH ₂) ₂ -OH	215	236 ± 3	230 ± 10	N/A	N/A	N/A	189 ± 2	181 ± 3
PVMS-S-(CH ₂) ₆ -OH	208	228 ± 12	210 ± 20	N/A	N/A	N/A	188 ± 2	180 ± 10
PVMS-S-(CH ₂) ₁₁ -OH	284.5	240 ± 40	270–290 ^g	306 ± 7	303 ± 9	300–320	189 ± 8	201 ± 5
PVMS-S-(CH ₂) ₂ -CH ₃		190 ± 2					162 ± 2	
PVMS-S-(CH ₂) ₁₁ -CH ₃	210		265 ± 5			290–300		140 ± 5

^aGlass transition. ^bMelting point. ^cFrom raw data at 1 Hz. ^dDetermined by extrapolating to $\tau = 100$ s. ^eFrom raw data at 100 Hz to 10 kHz. ^fFrom raw data at 100 Hz. ^gThe dominant feature in the DRS spectra was the peak at T_m . T_g was most clearly observed in aged samples.

dynamics of the larger system (e.g., the segmental dynamics related to the T_g of the substituted network) may affect responsiveness. Beyond the structure-response correlations pertaining to this specific system, these observations are also beneficial for developing rational design strategies for the larger class of stimulus-response surfaces consisting of polymer chains anchored to an underlying substrate.²

We will examine six polymer networks whose molecular parameters are summarized in Table 1. Those include: PVMS, PVMS-S-(CH₂)₂-OH, PVMS-S-(CH₂)₂-CH₃, PVMS-S-(CH₂)₆-OH, PVMS-S-(CH₂)₁₁-OH, and PVMS-S-(CH₂)₁₁-CH₃. Data from poly(dimethylsiloxane) (PDMS) networks are shown for comparison. The PVMS-S-(CH₂)_n-CH₃ species represent a special case of amphiphiles whose wettability decreases with increasing alkyl chain length. In this work, -CH₃ terminated networks will serve as a control to understand the differences in side-chain interactions due to the terminal -OH group.

II. Experimental Methods

Substrate preparation of modified PVMS networks and the experimental details of the static and dynamic contact angles have been previously reported.^{5,6} Elastomeric PVMS network

substrates were synthesized by following an alkoxy-cure method of PVMS ($M_n \approx 40$ kDa) through end-group cross-linking as described elsewhere.⁷ The storage modulus of the PVMS networks was measured to be $\approx 8 \times 10^4$ Pa after Soxhlet extraction using toluene for at least 48 h followed by drying at 75 °C under 30 mmHg vacuum. The vinyl moieties on PVMS were subsequently saturated via azobis(isobutyronitrile)- (AIBN)-initiated thiol-ene radical addition of HS-(CH₂)_n-OH ($n = 2, 6,$ and 11).⁸ After the reaction, the PVMS-S-(CH₂)_n-OH samples were re-extracted, dried, and stored in a low-humidity chamber. Experiments using infrared spectroscopy in the attenuated reflection mode confirmed that the grafting density of S-(CH₂)_n-OH was approximately equal in each sample.

Dynamic Mechanical Thermal Analysis (DMTA). DMTA was performed using a TA Instrument Q800 operating with single cantilever geometry. The dried polymer films were cut into approximately $25 \times 10 \times 1.5$ mm³ rectangles. Storage modulus (E'), loss modulus (E''), and loss tangent ($\tan \delta$) were recorded at a heating rate of 3 °C/min from -150 to +130 °C and at a test frequency of 1 Hz. The amplitude was set to be within the linear viscoelastic regime.

Differential Scanning Calorimetry (DSC). DSC was performed using a TA Instrument Q100. Two runs were carried out for each sample in the range of -80 to +130 °C with a heating rate of 3 °C/min under a nitrogen atmosphere. The glass

transition (T_g) values were determined as the onset points from the second scans if applicable. The melting point (T_m) was taken as the maximum of the endothermic peak.

Dynamic Relaxation Spectroscopy (DRS). DRS utilized a highly sensitive Andeen–Hagerling capacitance bridge operating at 50 Hz–20 kHz. Samples were mounted onto planar interdigitated electrodes, which enabled dielectric measurements on small amounts of material. This technique has been utilized previously for dielectric measurements on self-assembled monolayers⁹ and polymers.¹⁰ We specifically chose the narrow-band, highly sensitive technique, rather than conventional broad-band dielectric spectroscopy, so that we could measure small volumes of material from the same samples used for wettability measurements.

DRS Analysis. Dielectric relaxation spectroscopy utilizes the sample as a dielectric within a capacitor and measures the complex dielectric constant ($\epsilon^* = \epsilon' - i\epsilon''$) under application of an AC electric field¹¹ at frequency ω . The output of the precision bridge used in these experiments is capacitance (C) and $\tan \delta$ measured as a function of frequency and temperature. $C = A\epsilon'$, where A is a geometrical factor related to the size and shape of the capacitor, whereas $\tan \delta = \epsilon''/\epsilon'$. Ionic backgrounds were modeled as $\tan \delta = (A/T) \exp(-E_i/kT)/\omega^s$, where A is a constant related to the DC conductivity, the exponential term reflects the temperature dependence of ionic carriers with a characteristic barrier E_i , and s is dependent on the nature of ionic diffusion and can vary from 0 to 1.^{12,13}

The step in the capacitance or the more easily observed peak in $\tan \delta$ at $1/\tau = \omega$ allows for determination of τ (the characteristic relaxation time or average time between reorientation events) as a function of temperature for a particular applied field frequency ω .^{11,12} This temperature dependence can then be fitted to the Arrhenius form, $1/\tau = \omega_0 \exp(-\Delta U/kT)$ to determine ω_0 , the attempt or libration frequency and ΔU the barrier to reorientation. For independent or noninteracting relaxations, where the Arrhenius form is appropriate, this analysis yields physically interpretable values (e.g., $\omega_0 \approx 10^{13} - 10^{15}$ rad/s); however, for interacting objects where the barrier (ΔU) changes with temperature, particularly for glassy relaxations, fitting with the Arrhenius form produces artificially high apparent values for ω_0 and ΔU . In this case, a more appropriate analysis utilizes the empirical Vogel–Fulcher–Tammann (VFT) form,^{14–16} $1/\tau = \omega_0 \exp[-B/(T - T_0)]$, where the argument of the exponent provides a barrier that increases with decreasing temperature (B is a constant). T_0 is a temperature below which all motion has ceased and in our fits, ω_0 is held at 10^{14} rad/s to reduce the number of free parameters. Glassy relaxations are quantified by defining T_g as the temperature at which $\tau = 100$ s,¹⁷ determined by fitting the measured τ versus T with the VFT form and extrapolating to large τ .

In this work, we plotted $\ln(1/\tau)$ versus $1/T$ and fit with either the Arrhenius or VFT forms as appropriate to determine either ΔU , the barrier to rotation, or T_g for glassy relaxations. Ionic backgrounds were removed from the data for PVMS–S–(CH₂)₂–CH₃ and PVMS–S–(CH₂)₆–OH samples. For relaxations within interacting side-chains, which are not a glassy system *per se*, but which display an elevated apparent ω_0 value, we utilized a Starkweather analysis. Starkweather argued that there are significant entropy changes in cooperative relaxations, in contrast with $\Delta S = 0$ for a simple independent motion, and that this value could be used to quantify the level of interaction in different systems.¹⁸ In this analysis, the Arrhenius form is used to fit the data and the observed activation energy ΔU and peak position T' are transformed into a ΔS value as: $\Delta S = \Delta U - k[1 + \ln(k/2\pi h) + \ln(T'/f)]$, where T' is the temperature at which the relaxation is f Hz. In our case, we utilized ΔU values from Arrhenius fits, and performed the Starkweather analysis at 1 kHz, in the middle of our experimental frequency range.

III. Results

A. Macroscopic Response. The macroscopic response of the substituted PVMS networks was characterized previously

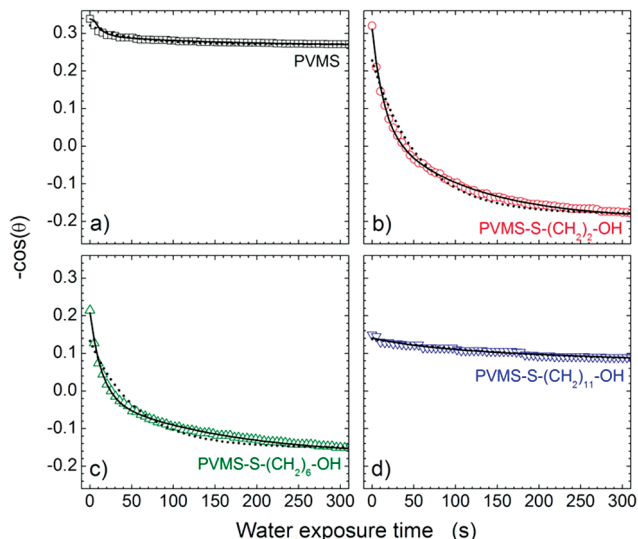


Figure 2. Time dependence of the negative cosine of the contact angle (θ) measured by DCA (second cycle) for (a) PVMS (black squares), (b) PVMS–S–(CH₂)₂–OH (red circles), (c) PVMS–S–(CH₂)₆–OH (green up-triangles), and (d) PVMS–S–(CH₂)₁₁–OH (blue down-triangles). The dotted and solid lines represent the best fit to eqs 1 and 2, respectively, as described in the text.

by studying the cycling between hydrophobic (dry) and hydrophilic states (wet) states by dynamic contact angle (DCA). The degree of wettability change and the rate of response, i.e., the variation of the water contact angle (θ) with time (τ), were shown qualitatively to decrease with increasing the number of methylene units (n) in the mercaptoalkanol hydrocarbon spacer. Moreover, long linkers were seen to cocrystallize locally thus freezing the conformation until it was relieved by heating the sample above the melting point of the alkane crystallites.^{5,6} The open symbols in Figure 2 depict representative examples of such wettability changes recorded for PVMS (squares), PVMS–S–(CH₂)₂–OH (circles), PVMS–S–(CH₂)₆–OH (up-triangles), and PVMS–S–(CH₂)₁₁–OH (down-triangles). These data reveal that while PVMS exhibits a relatively modest, but fast, wettability change, PVMS–S–(CH₂)₂–OH and PVMS–S–(CH₂)₆–OH display similar reorganization kinetics, along with a larger change in wetting, upon transitioning from a hydrophobic to a hydrophilic environment. PVMS–S–(CH₂)₁₁–OH does not exhibit this large change in wettability during the cycling behavior even before the side-chains crystallize.

We extend these observations by quantitatively interpreting the DCA data. We first analyzed the DCA data by fitting each cycle individually to the first order exponential decay:

$$-\cos(\theta) = A + B_1 \exp(-\beta_1 t) \quad (1)$$

In eq 1, A , B_1 , and β_1 were used as fitting parameters; β_1 represents an inverse of a characteristic relaxation time. We averaged the fitting exponents from runs 2–10 (excluding run number 1 because of unknown sample history during preparation) for PVMS, PVMS–S–(CH₂)₂–OH, and PVMS–S–(CH₂)₆–OH, and cycles 2–4 for PVMS–S–(CH₂)₁₁–OH (after the fourth cycle the structure froze because of local cocrystallization among –(CH₂)₁₁–OH). The dotted lines in Figure 2 denote the values of $-\cos(\theta)$ as a function of time obtained by the best fits to eq 1. While the fits to PVMS and PVMS–S–(CH₂)₁₁–OH were satisfactory ($R^2 > 0.98$), the first order exponential decays did not capture accurately the trends observed in the PVMS–S–(CH₂)₂–OH

and PVMS-S-(CH₂)₆-OH specimens. We then reanalyzed the DCA data by fitting to the second order exponential decay:

$$-\cos(\theta) = A + B_1 \exp(-\beta_1 \tau) + B_2 \exp(-\beta_2 \tau) \quad (2)$$

The solid lines in Figure 2 represent the best fits to eq 2 with A , B_1 , β_1 , B_2 , and β_2 being used as fitting parameters. The quality of the fits improved considerably for all data sets. In Figure 3 we plot the values of the decay coefficients β_1 (closed symbols) and β_2 (open symbols) for all substrates. From the data in Figure 3, it is apparent that β_1 decreases systematically with increasing n , while β_2 remains relatively constant for all specimens. Recalling that β_j is inversely related to

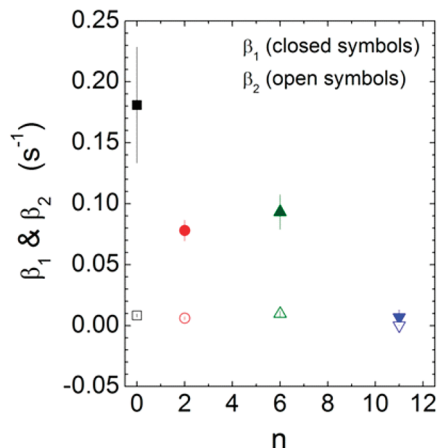


Figure 3. Coefficients in the 2nd order exponential decay function (β_1 : solid symbols, β_2 : open symbols) for PVMS (black squares), PVMS-S-(CH₂)₂-OH (red circles), PVMS-S-(CH₂)₆-OH (green up-triangles), and PVMS-S-(CH₂)₁₁-OH (blue down-triangles) as a function of the number of methylene units in PVMS-S-(CH₂)_n-OH.

a relaxation time and assuming that the second order exponential decay is a physically reasonable functional form, there are two superimposed processes that govern wettability changes in the specimens: a fast one (given by β_1) and a slower one (given by β_2). We will return to the issue of second order exponential decay later in the Discussion.

B. Characterization of Molecular-Level Motion. DSC scans for PVMS, PVMS-S-(CH₂)₂-OH, PVMS-S-(CH₂)₆-OH, and PVMS-S-(CH₂)₁₁-OH are shown in Figure 4; the results are also summarized in Table 1. The first three compounds exhibit a clear step-change in the heat

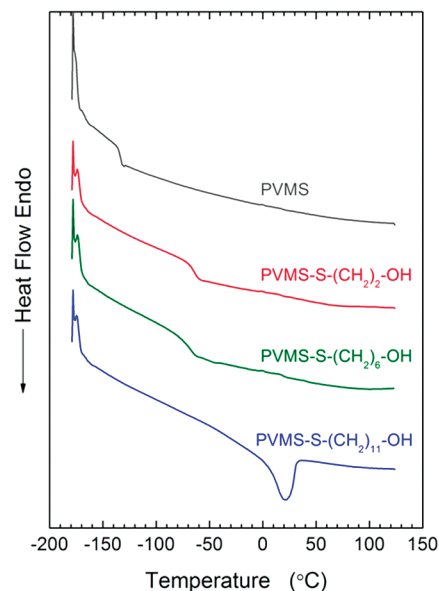


Figure 4. DSC measurements for PVMS and PVMS-modified substrates. The heating rate was 3 °C/min, see text for details.

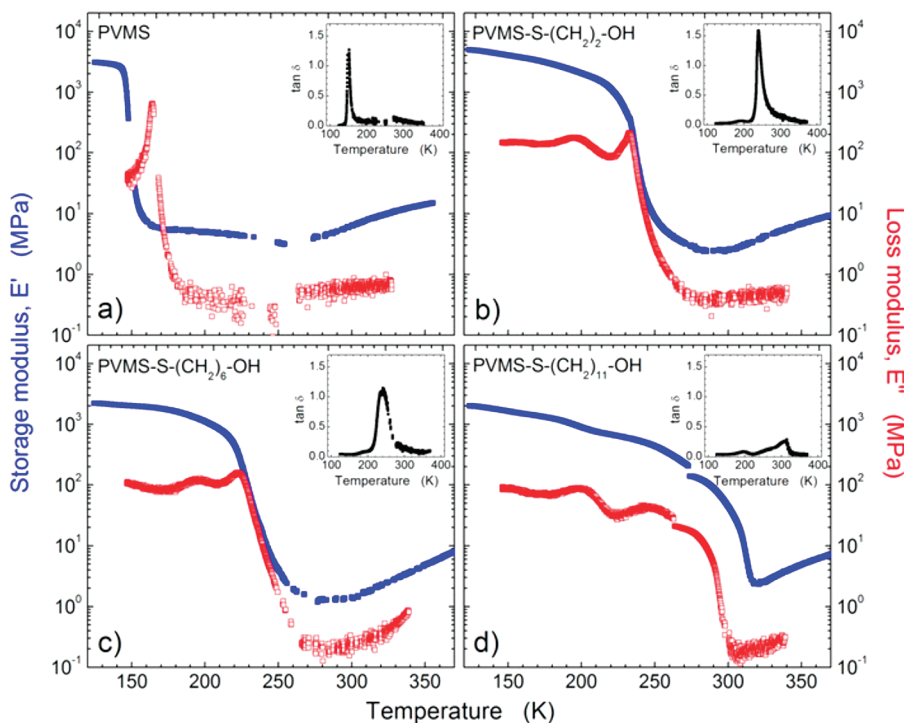


Figure 5. DMTA data for PVMS and PVMS-mercaptanol modified substrates depicting the storage (left ordinate, closed blue symbols) and loss (right ordinate, open red symbols) moduli, E' and E'' , respectively, for PVMS (a), PVMS-S-(CH₂)₂-OH (b), PVMS-S-(CH₂)₆-OH (c), and PVMS-S-(CH₂)₁₁-OH (d). Temperature ramps were performed at a heating rate of 3 °C/min and at 1 Hz. Amplitude was set within the linear viscoelastic regime. The inset graphs depict $\tan \delta$, i.e., $\tan(E''/E')$.

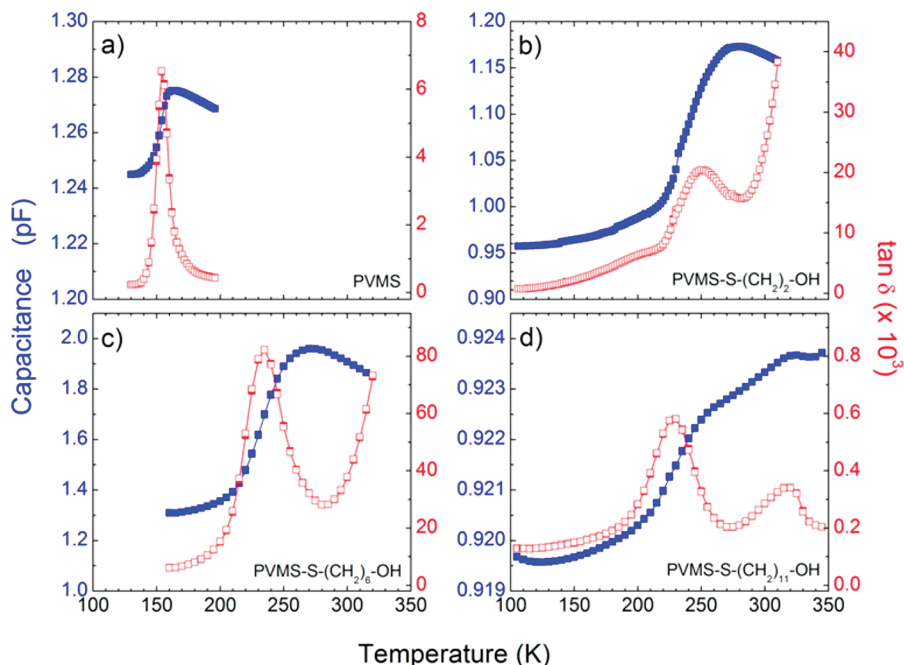


Figure 6. Capacitance (left ordinate, blue solid symbols) and $\tan \delta$ (right ordinate, red open symbols) from DRS measurements at 10 kHz for PVMS (a), PVMS-S-(CH₂)₂-OH (b), PVMS-S-(CH₂)₆-OH (c), and PVMS-S-(CH₂)₁₁-OH (d).

flow output at the glassy transition state plateau. The resultant T_g values are given in Table 1. Data from PVMS-S-(CH₂)₁₁-OH reveal a melting transition that results in a distinct endothermic peak superimposed near the glass transition feature. We have previously reported on crystallization of PVMS-S-(CH₂)₁₁-OH.^{5,6}

DMTA data for PVMS, PVMS-S-(CH₂)₂-OH, PVMS-S-(CH₂)₆-OH, and PVMS-S-(CH₂)₁₁-OH are shown in Figure 5. The largest step change in elastic modulus E' , maxima in loss modulus E'' , and maxima in $\tan \delta$ ($E' \cong 3G'$, $E'' \cong 3G''$, and $\tan \delta = E''/E'$) indicates the position of the α transition (T_α), which is assigned as the glass transition temperature (T_g).^{19,20} PVMS exhibits a clear transition at ≈ 150 K associated with the T_g . In PVMS-S-(CH₂)₂-OH and PVMS-S-(CH₂)₆-OH, the most dramatic change corresponds to the T_g ; these values match well with those from DSC (cf. Table 1). In addition, a smaller secondary relaxation appearing at a temperature below T_g is present. The locations of these features (labeled as β) are also summarized in Table 1. The presence of crystallinity complicates the spectrum of PVMS-S-(CH₂)₁₁-OH. In this case, the highest temperature feature is due to melting. In addition, there is a feature associated with the glass transition as well as a secondary (β) relaxation below T_g . In addition to single frequency data, DMTA measurements were taken at a range of frequencies for the PVMS and PVMS-S-(CH₂)₁₁-OH samples. The α and β relaxations in PVMS-S-(CH₂)₂-CH₃ were also studied by DMTA (cf. Table 1).

DRS spectra at 10 kHz for PVMS, PVMS-S-(CH₂)₂-OH, PVMS-S-(CH₂)₆-OH, and PVMS-S-(CH₂)₁₁-OH are plotted in Figure 6. The trends in the DRS data follow those in the DMTA results. For PVMS a single relaxation is observed which corresponds to the α relaxation in DMTA; whereas both α and sub- T_g (β) relaxations are observed in the PVMS-S-(CH₂)_n-OH samples. At the frequency utilized for the data depicted in Figure 6, the β and α relaxations are merged; however, they can be seen more clearly in Figure 7, which displays $\tan \delta$ for PVMS-S-(CH₂)₂-OH at frequencies

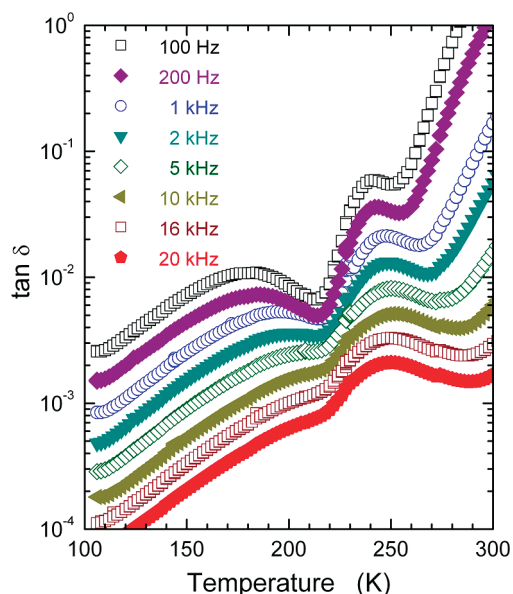


Figure 7. Dissipation factor ($\tan \delta$) as a function of temperature for PVMS-S-(CH₂)₂-OH. The logarithmic scale enables tracking of the low temperature relaxation. An arbitrary y-axis offset was applied to each data set.

varying from 100 Hz to 20 kHz. Figure 8 summarizes the sub- T_g (β) relaxations for PVMS-S-(CH₂)₂-OH, PVMS-S-(CH₂)₆-OH, and PVMS-S-(CH₂)₁₁-OH, and PVMS-S-(CH₂)₁₁-CH₃. The α peak for PVMS-S-(CH₂)₂-OH and PVMS-S-(CH₂)₆-OH is shown for comparison.

For PVMS-S-(CH₂)₂-OH, the lower temperature (β) DRS peak is the smaller in amplitude, and appears at 180 to 210 K for applied frequencies ranging from 100 Hz to 5 kHz. At higher frequencies, the smaller β peak shifts into the larger amplitude, higher temperature α peak, and is no longer clearly distinguishable. The β peak positions form a straight line on an Arrhenius plot (see Experimental Methods), with

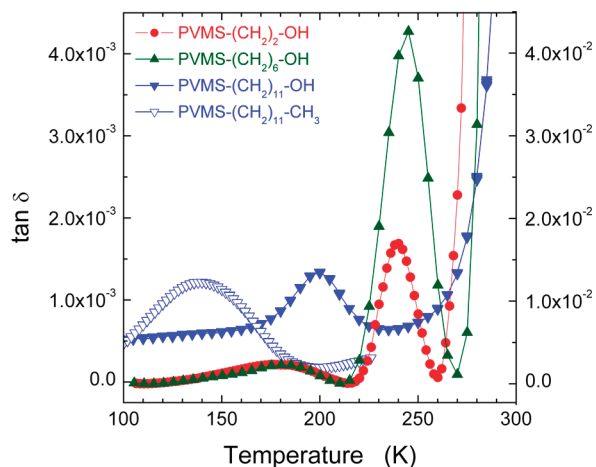


Figure 8. Dissipation factor for (right ordinate) PVMS-S-(CH₂)₂-OH (filled red circles), PVMS-S-(CH₂)₆-OH (filled green up-triangles), and (left ordinate) PVMS-S-(CH₂)₁₁-OH (filled blue down-triangles), PVMS-S-(CH₂)₁₁-CH₃ (open blue down triangles) at 100 Hz. A background due to ionic conductivity has been removed from each sweep. This sweep of PVMS-S-(CH₂)₁₁-OH data displays a melting peak at ≈ 315 K. The higher temperature peak for PVMS-S-(CH₂)₂-OH and PVMS-S-(CH₂)₆-OH is associated with T_g .

slightly elevated attempt frequency of $\approx 10^{16}$ rad/s. and a barrier of 10.9 ± 0.8 kcal/mol. For the 100 Hz to 20 kHz frequency range, the higher amplitude and temperature α peak occurred at 240–250 K with only a small peak shift as a function of frequency. Such small peak shifts with frequency change are consistent with “glassy” or strongly interacting relaxations, which reflect the very rapid change in the rate of the molecular motion over very small changes in temperature. Thus, we assign this relaxation as associated with segmental motion and the glass transition.

The α DRS peak for the -(CH₂)₆-OH samples appears at similar temperatures as the -(CH₂)₂-OH equivalent, ranging from 245 to 270 K, for 100 Hz to 20 kHz. As in PVMS-S-(CH₂)₂-OH, the lower temperature peak in PVMS-S-(CH₂)₆-OH DRS data was smaller in amplitude than the α -relaxation. At 100 Hz, this β peak occurred at the same location as the -(CH₂)₂-OH (180 K), before shifting into the higher temperature α feature at frequencies above 500 Hz.

For PVMS-S-(CH₂)₁₁-OH, two peaks corresponding to the β and melting relaxations were observed in most specimens. The data in Figure 5d are representative. The lower temperature (β) peak had the larger amplitude and occurred at 200–230 K, for 100 Hz to 20 kHz. For aged samples of -(CH₂)₁₁-OH, the melting peak was not present and an α relaxation associated with the T_g was observed.

PVMS-S-(CH₂)₁₁-CH₃ showed a high temperature peak in the dielectric relaxation data occurring at ≈ 290 –300 K, which had characteristics associated with a melting transition (including a discontinuous change in capacitance at T_m). It is not uncommon for side-chains with $n = 11$ to crystallize, even without a terminal -OH group. A relaxation due to T_g was observed in the capacitance (enhanced by taking a derivative with respect to temperature). T_g , T_m , and β peak locations from DRS for the C₁₁ substituted networks appear in Table 1.

IV. Discussion

A. Comparison of T_g as a Function of Structural Changes. DMTA and DRS data for PVMS networks were consistent in displaying a sharp dispersing peak varying in location

from 145 to 155 K from 0.1 Hz to 20 kHz. Analysis of the data (see Experimental Methods) resulted in an estimated $T_g = 140 \pm 5$ K, which is consistent with the T_g value recorded by DSC. These values match the T_g of 143 K reported for linear PVMS.²¹ Thus, the cross-linking employed to form the network does not appear to alter T_g , and the PVMS backbone retains its highly flexible properties. This observation also holds for PDMS (see Table 1; for comparison linear T_g for PDMS: 145–150 K, depending on crystalline fraction²²).

From the PVMS-S-(CH₂)₂-OH DRS data, $T_g = 230 \pm 10$ K, a nearly 100 K increase from the PVMS. This T_g is consistent with the DMTA value of 236 ± 3 K at 1 Hz. The DSC T_g of 215 K also displays a similar increase over the PVMS network value (148 K). This indicates that the T_g has been increased significantly due to the presence of the -S-(CH₂)₂-OH side-chains. Dramatic changes in PVMS glass transition temperatures (≈ 50 –200 K) have been observed previously when substituting bulky side-chains, which presumably hinder motion of the flexible siloxane backbone.²¹ The increase in T_g indicates that there are sufficient steric interactions between the pendent groups or between the pendent groups and backbone to alter the backbone dynamics.

The α DRS peak for the -(CH₂)₆-OH samples appeared at similar temperatures as the -(CH₂)₂-OH equivalent, with a T_g of 210 ± 20 K. The value from DSC was 208 K. These T_g values overlap with the corresponding results for -(CH₂)₂-OH. The DMTA data are also similar for the two materials with a primary peak centered at ≈ 230 –240 K (1 Hz). While this lack of change in T_g when transitioning to the longer chain may be attributed to the well-known plasticizing effect of alkyl chains of moderate length,²³ it could alternatively be caused by a slight variation of the -S-(CH₂)_n-OH loading in the PVMS-S-(CH₂)_n-OH network. Though, as we note in the Experimental Methods, the loading of -S-(CH₂)_n-OH inside the PVMS-S-(CH₂)_n-OH network appeared to be approximately the same, as revealed by IR spectroscopy.

PVMS-S-(CH₂)₁₁-OH displayed T_m features in the range 299–311 K (DSC) and 294–312 K (DMTA). Evidence of melting (often associated with a large discontinuous change in the ϵ'' or, equivalently, capacitance) was observed in the dielectric data at 300–320 K. For most DRS samples, this was the dominant high temperature relaxation and no peak associated with the glass transition was observed. For some samples, particularly those that had been aged at ambient conditions for a year or so after fabrication, a peak ranging from 282 to 287 K (320 Hz to 20 kHz) was observed. This results in an estimated T_g in the 270–290 K range, which is consistent with that observed in the DSC (284.5 K). Features in DMTA associated with the α relaxation varied in position from 240 to 270 K. These T_g values are significantly higher than for the networks with shorter pendant groups, indicating that the backbone dynamics are further constrained by the longer chains. Generally the DMTA and DS data from -(CH₂)₁₁-OH samples exhibited more complex structure and sample to sample differences than the other materials, which is consistent with a semicrystalline material.

In order to study the role of the terminal group in modifying dynamics within the network, PVMS-S-(CH₂)₂-CH₃ and PVMS-S-(CH₂)₁₁-CH₃ were also investigated. In a DMTA study of PVMS-S-(CH₂)₂-CH₃ and PVMS-S-(CH₂)₂-OH, the T_g dropped significantly from 236 ± 3 K to 190 ± 3 K without the -OH group present (Table 1). This value is still larger than the T_g for the PVMS network without pendent groups (≈ 150 K). The -(CH₂)₁₁-

analogues were studied by DRS. When comparing the $-(\text{CH}_2)_{11}-\text{CH}_3$ pendent group with the more polar $-(\text{CH}_2)_{11}-\text{OH}$, the T_g only decreased slightly to 265 ± 5 K (compared with $-(\text{CH}_2)_{11}-\text{OH}$ estimate of 270–290 K). Interestingly, the DSC measurement of T_g shows a much larger decrease from 285 to 210 K. These results indicate that both the length and termination of the pendent group affect the glass transition temperature; that is, that pendent–pendent or pendent–backbone interactions determine the effective T_g .

B. Sub- T_g Relaxations. The low-temperature (β) peak in the PVMS–S– $(\text{CH}_2)_2$ –OH DRS data is consistent with rotation within the pendent-group alkyl chains. Relaxations due to local motions within side-chains often follow Arrhenius dynamics. Side-chain peaks are generally smaller in amplitude than those associated with T_g (α relaxations) and appear at sub- T_g temperatures. There exists a well-known local relaxation in the 120–150 K range (for 100 Hz) that is associated with alkyl side groups^{24–27} and has also been observed in alkyl self-assembled monolayers.^{9,28} Previous workers have assigned this relaxation to a crankshaft-like motion where two gauche defects alternate in orientation without significantly changing the average volume taken up by the chain.²⁹ The presence of the polar –OH group and/or polarized bonds near –S– would enable dielectric observation of these motions. Although the exact nature of the relaxation is still debated,^{26,27} it is mostly independent of the backbone structure²⁵ and thus a common feature for polymers with alkyl side-chains. A similar local relaxation occurs in polyethylene (named the PE- γ relaxation in that case).^{28,29} The barriers observed for this PE- γ relaxation are generally ≈ 6 –7 kcal/mol. However, in side-chain polymers this relaxation has been observed at higher temperature (larger barriers) when interchain interactions are present.³⁰ Our results are consistent with the presence of a PE- γ -like relaxation, with an elevation in barrier (to 10.9 ± 0.8 kcal/mol) resulting from interchain interactions due to the –OH group. Sub- T_g or side-chain motions are not generally observable in DSC, which is consistent with this assignment.

Comparing peak positions for the β relaxation from DMTA and DRS (190 K at 1 Hz, and 180 K at 100 Hz) it appears that the barrier is lower in the dielectric case. This has previously been observed for other local relaxations.^{26,31} In that case, the authors argued that the coupling between the electric field and the dipole was direct; whereas the coupling between the applied mechanical stress and the side-chains was more indirect, and therefore associated with a higher barrier. Thus, the two techniques measured different responses. In our materials only the terminal –OH group or a polarized bond near the thiolene attachment need respond to provide a dielectric signal, which may have slightly different dynamics than a relaxation in the interior of the chain.

Comparing the response of $-(\text{CH}_2)_2$ –OH and $-(\text{CH}_2)_6$ –OH pendent groups, we find that the DMTA data is similar for both, with peaks at ≈ 190 K. This similarity also holds for the DRS data (180 K for 100 Hz). Considering the constraints on the data due to peak merging, we conclude that the relaxation is similar for –S– $(\text{CH}_2)_2$ –OH and –S– $(\text{CH}_2)_6$ –OH pendent groups.

In contrast, the β dielectric relaxation in PVMS–S– $(\text{CH}_2)_{11}$ –OH (DRS) was shifted to higher temperatures (200 K at 100 Hz). DMTA data showed an equivalent β relaxation in the range of 180–197 K at 1 Hz. These peak positions are higher in temperature than for the shorter side-chains, indicating slower dynamics. Analysis of the DRS data revealed that the $-(\text{CH}_2)_{11}$ –OH pendent groups have significant interaction, with an elevated apparent attempt

frequency of $\approx 10^{20}$ rad/s and an effective barrier of 16 ± 0.8 kcal/mol. A Starkweather analysis (see Experimental Methods) showed $\Delta S = 115 \pm 32$ J/mol/K, compared to $\Delta S = 60 \pm 10$ J/mol/K for $-(\text{CH}_2)_2$ –OH. Thus, we conclude that the $-(\text{CH}_2)_{11}$ –OH chains are significantly more interacting than the $-(\text{CH}_2)_2$ –OH or $-(\text{CH}_2)_6$ –OH side-chains. This is consistent with previous observations of crystallization of the $-(\text{CH}_2)_{11}$ –OH side-chains. Although this relaxation has interacting dynamics, it did not appear in the DSC sweep, which is representative of an interacting side-chain relaxation rather than a glass or melting transition.

The amplitude of the DRS β relaxation PVMS–S– $(\text{CH}_2)_{11}$ –OH increased with increasing temperature (higher measurement frequency) in contrast to the short side-chain network data where the amplitude was constant. Such an increase indicates that the number of units participating in the relaxation is increasing with temperature.^{32,33} This could occur because the side-chain relaxation is localized in the amorphous regions, and the amorphous fraction is increasing with temperature. In addition, an asymmetrical potential surface could explain this result. In thermally activated hopping, any reorienting group is hindered by a potential surface with more than one accessible minimum, i.e., reorientation involves transition from one minimum to another over an effective barrier ΔU . However, if the energy difference between the minima, B' , is sufficiently large (compared to kT), a particular unit will remain frozen in a single well, and thus not reorient. For a distribution of B' values, as the temperature increases, more units will be available for reorientation. Thus, in general, an increasing signal with temperature is associated with asymmetrical potential surfaces. Such asymmetry can occur when strong local interactions are present, which is consistent with the significant interactions between the $-(\text{CH}_2)_{11}$ –OH pendent groups.

The β transition was also studied for methyl-terminated pendent groups. The relaxation in PVMS–S– $(\text{CH}_2)_2$ – CH_3 shifts downward from that in PVMS–S– $(\text{CH}_2)_2$ –OH, indicating faster dynamics (DMTA measurements, Table 1). This occurs in the $-(\text{CH}_2)_{11}$ – system as well, as studied by DRS. In that case, the peak shifted downward significantly (140–170 K, from 100 Hz to 20 kHz), and displayed a resultant barrier to rotation of 7.7 ± 0.5 kcal/mol (compared to 16 kcal/mol for the C_{11} –OH networks). Starkweather analysis revealed $\Delta S = 34 \pm 12$ J/mol/K, indicating a significant drop in interaction compared with the $-(\text{CH}_2)_{11}$ –OH case, and similar or lower interactions as within the side-chains of PVMS–S– $(\text{CH}_2)_2$ –OH. Thus, the presence of the –OH group increases the effective barrier (in both the C_2 and C_{11} cases), and in the absence of the –OH group, the barrier to rotation and peak location of the β -motion are similar to γ -PE relaxation in alkyl side-chain polymers. This confirms our assignment of the relaxation.

C. Relationship between T_g and the Macroscopic Responsiveness. Generally, the three techniques (DSC, DRS, and DMTA) agree in their determination of T_g within the experimental error. Cross-linking to form the network does not affect the flexibility of the PVMS backbone; however upon grafting of the –S– $(\text{CH}_2)_2$ –OH pendent group T_g increases by > 60 K. The T_g of PVMS–S– $(\text{CH}_2)_{11}$ –OH is significantly higher than that of the other substituted systems, indicating that the strong interactions among the –S– $(\text{CH}_2)_{11}$ –OH groups hinder substantially the motion of the siloxane backbone.

The trends in T_g match qualitatively with the response rate detected in the DCA experiments at room temperature. Namely, the response rate at room temperature of PVMS–S– $(\text{CH}_2)_n$ –OH increases with decreasing T_g . This

trend is not unexpected as materials farther above their glass transition temperature should possess faster dynamics. To that end, PVMS exhibits the fastest response rate, followed by PVMS-S-(CH₂)₂-OH and PVMS-S-(CH₂)₆-OH and finally, PVMS-S-(CH₂)₁₁-OH exhibits the most sluggish response.

Recall that earlier in the paper we pointed out that the DCA experimental data could not be fitted satisfactorily with a simple exponential decay function. In contrast, a second order exponential decay, i.e., eq 2, provided a better fit. Interestingly, the decay coefficients β_1 and β_2 used in eq 2 plotted in Figure 3 exhibit two distinct trends. While β_1 decreases steadily with increasing the length of the methylene spacer, β_2 is independent of the size of the pendent group. If the network T_g is well correlated with the response time, as reflected in β_1 , this would indicate that the segmental dynamics control the motion of the pendent group through the network. The time scale of segmental fluctuations is given by τ micro, the average time between reorientation events, the value of which (at room temperature) can be estimated from the DRS data. This τ micro should be related to the macroscopic response time τ macro = $1/\beta_1$ from the analysis of the dynamic contact angle (cf. Figures 2 and 3). Thus, in order to further correlate microscopic and macroscopic motion, we fit our DRS relaxation data (see Experimental Methods), and then extrapolated this fit to estimate τ micro at room temperature where the DCA measurements were taken. This is similar to the extrapolation utilized to determine T_g . As already discussed, these T_g values (listed in Table 1) agree well with data from DSC and DMTA data taken at 1 Hz, which indicates that the fits are appropriate.

Since many segmental fluctuations would be required for a single -S-(CH₂)_n-OH group to emerge from the surface upon application of water, we expect the microscopic and macroscopic relaxation times to vary by many orders of magnitude. The τ micro values for -S-(CH₂)₂-OH and -S-(CH₂)₆-OH were similar whereas the value for -S-(CH₂)₁₁-OH was about ten times larger. These ratios are similar to those for the equivalent $1/\beta_1$ values. Comparing the four τ pairs (for the different network types) we find τ macro $\approx 1 \times 10^9$ τ micro. We conclude that there is a good qualitative correlation between these two τ estimates, which result from completely isolated and independent measurements of the samples properties.

We could find no correlations between the slower macroscopic relaxation time (given by the inverse of β_2) and any other physical quantity measured. The slower process is unlikely to originate from the relaxations of the side groups because those relaxations are likely faster than or have similar dynamics to the segmental motions at room temperature. Moreover, the process responsible for β_2 should be independent of the molecular architecture of the silicone elastomer chain. Unlike other analytical methods employed in this work, which probe the bulk properties of the system, DCA is sensitive only to the surface and near subsurface region of the network. We thus tentatively associate the slower relaxation process observed in the DCA data with the rearrangement of subsurface chains that move when the macromolecules present at the surface reorganize. This process may thus be associated tentatively with the overall mobility of the networks that would depend on the average molecular weight between the cross-link points; those were exactly the same in all specimens studied. In order to test this hypothesis, experiments similar to the one described here would have to be carried out using networks that possess different cross-link densities.

D. Relationship between Pendant Group Interactions and T_g . Generally, longer pendent groups and stronger interactions between the pendent groups (as exemplified by the -(CH₂)₁₁-OH case) leads to an increase in T_g , as the steric and/or dipolar interactions between the chains limit the flexibility of the PVMS backbone. These interchain interactions also affect, and are reflected in, the β relaxation. Thus, although the β relaxation within the pendent groups is not directly related to the responsiveness of the networks, observing its dynamics enhances our understanding of the pendent group interactions that lead to a resultant network T_g , and thus a characteristic response time to applied stimulus.

The α relaxation results indicate that both steric and dipolar interactions can effect interchain or chain-backbone interactions and thus the stiffening of the PVMS network. For the short chain case, both effects appear distinctly important, as exhibited in the difference in T_g values for the -(CH₂)₂-OH and -(CH₂)₂-CH₃ networks. For the longer chain, the situation is less clear, in part due to the complications of measuring a semicrystalline material under a variety of conditions. It may be that steric interactions between the side-chains are the dominant effect for long chains, and thus primarily responsible for the increase in T_g , explaining why the two -(CH₂)₁₁- pendent groups result in a similar T_g .

The polarity of the pendent group is important because it determines the *magnitude* of the response. As outlined above, the flexibility of the network, through which the pendent group must travel, affects the response *time*. For this particular set of networks, these two effects are correlated. Because the PVMS backbone is highly flexible, interactions between the pendent groups stiffen the network, raising T_g , and slowing the response time. Increasing the difference in hydrophobicity between the two switching groups (the -CH₃ and the vinyl or -OH pendent terminus), creates a larger drive (energy difference) to respond to a change in environment (application of water or air). However, rather than enhancing the response time (due to the increased driving force) the increased polarity of the pendent groups causes interactions which stiffens the network, thus (counterintuitively) slowing down the response.

These results reveal the delicate balance needed in the design of such responsive networks. For instance, decreasing the density of pendent groups would significantly decrease interchain interactions and thus allow for groups with stronger polarity without significant increases in T_g . However, a lower density of pendent groups would also decrease the magnitude of the response. An ideal design will utilize an optimal density and polarity of pendent groups to maximize both response size and speed.

V. Conclusions

By combining dielectric, calorimetric, and mechanical measurements we observed both intrapendent and PVMS-backbone relaxations within stimulus-responsive PVMS networks. T_g was not affected by network formation but increased by ≈ 40 K with introduction of the -S-(CH₂)₂-CH₃ pendent, and another 25–40 K for the polar analogue, i.e., -S-(CH₂)₂-OH. T_g values for PVMS-S-(CH₂)₂-OH and PVMS-S-(CH₂)₆-OH were similar, but the T_g increased significantly (≈ 50 K) for the longer pendent group, i.e., -(CH₂)₁₁-OH and -(CH₂)₁₁-CH₃. Thus, as the pendent groups are altered, the network T_g changes, as the different groups constrained the siloxane backbone to differing degrees. This indicates that network dynamics can be tuned significantly ($\Delta T_g = 130$ K) by adjusting the size, shape, and polarity of the pendent groups.

β relaxations were also observed for all pendent groups, and were assigned to rotation within the pendent alkyl chain. Study of the β relaxation enabled an understanding of the changes in T_g as resulting from steric or dipolar interchain or chain-backbone interactions which stiffen the system.

For macroscopic responsiveness the pendent groups must travel through the PVMS network, thus the flexibility of the network appears to be one limitation to response time. For systems with significant interactions between the pendent groups, T_g is elevated and the response time is slow. These two effects may arise from the same source; namely, the increased interactions between pendent groups, which increase the rigidity of the entire system. When pendent groups are less interacting, some of the flexibility of the PVMS backbone is retained, and macroscopic response times approach that of the unsubstituted PVMS. Taken as a whole, these results indicate that a holistic approach, understanding both the driving forces and the intrinsic molecular motions within a system, is desirable for effective design of stimuli-responsive systems.

Acknowledgment. J.A.C.-W. and J.G. acknowledge the support through the Office of Naval Research, Grant No. N00014-08-1-0369. We thank Professor Saad Khan and Professor Russell Gorga for the generous use of their DSC and DMTA equipment.

References and Notes

- (1) Minko, S. *Polym. Rev.* **2006**, *46*, 397–420.
- (2) Cohen Stuart, M. A.; Huck, W. T. S.; Genzer, J.; Muller, M.; Ober, C.; Stamm, M.; Sukhorukov, G. B.; Szleifer, I.; Tsukruk, V. V.; Urban, M.; Winnik, F.; Zauscher, S.; Luzinov, I.; Minko, S. *Nature Mater.* **2010**, *9*, 101–103.
- (3) Luzinov, I.; Minko, S.; Tsukruk, V. V. *Prog. Polym. Sci.* **2004**, *29*, 635–698.
- (4) Luzinov, I.; Minko, S.; Tsukruk, V. V. *Soft Matter* **2008**, *4*, 714–725.
- (5) Crowe, J. A.; Genzer, J. *J. Am. Chem. Soc.* **2005**, *127*, 17610–17611.
- (6) Crowe-Willoughby, J. A.; Genzer, J. *Adv. Funct. Mater.* **2009**, *19*, 460–469.
- (7) Efimenko, K.; Crowe, J. A.; Manias, E.; Schwark, D. W.; Fischer, D. A.; Genzer, J. *Polymer* **2005**, *46*, 9329–9341.
- (8) Herczynska, L.; Lestel, L.; Boileau, S.; Chojnowski, J.; Polowinski, S. *Eur. Polym. J.* **1999**, *35*, 1115–1122.
- (9) Scott, M. C.; Stevens, D. R.; Bochinski, J. R.; Clarke, L. I. *ACS Nano* **2008**, *2*, 2392–2400.
- (10) Rotella, C.; Napolitano, S.; Wuebbenhorst, M. *Macromolecules* **2009**, *42*, 1415–1417.
- (11) McCrum, N. G.; Read, B. E.; Williams, G. *Anelastic and Dielectric Effects in Polymeric Solids*, Dover 1991 ed.; Wiley: London, 1967.
- (12) Horansky, R. D.; Clarke, L. I.; Winston, E. B.; Price, J. C. *Phys. Rev. B* **2006**, *74* (5), 054306.
- (13) Sidebottom, D. L.; Green, P. F.; Brow, R. K. *J. Non-Cryst. Solids* **1997**, *222*, 354–360.
- (14) Fulcher, G. S. *J. Am. Ceram. Soc.* **1925**, *8*, 339–355.
- (15) Tammann, G.; Hesse, W. Z. *Anorg. Allgem. Chem.* **1926**, *156*, 14.
- (16) Vogel, H. *Phys. Z.* **1921**, *22*, 645–646.
- (17) Angell, C. A. *Science* **1995**, *267* (5206), 1924–1935.
- (18) Starkweather, H. W. *Macromolecules* **1981**, *14*, 1277–1281.
- (19) Murayama, T. *Dynamic Mechanical Analysis of Polymeric Materials*; Elsevier Scientific Publishing Company: Amsterdam, 1978.
- (20) Ferry, J. D. *Viscoelastic Properties of Polymers*; John Wiley & Sons: New York, 1961.
- (21) Gupta, S. K.; Weber, W. P. *Macromolecules* **2002**, *35*, 3369–3373.
- (22) Lund, R.; Alegria, A.; Goitandia, L.; Colmenero, J.; Gonzalez, M. A.; Lindner, P. *Macromolecules* **2008**, *41*, 1364–1376.
- (23) Painter, P. C.; Coleman, M. M. *Essentials of Polymer Science and Engineering*; DEStech Publications: Lancaster, PA, 2009.
- (24) Diazcalleja, R. J. *J. Polym. Sci., Part B: Polym. Phys.* **1979**, *17*, 1395–1401.
- (25) Genix, A. C.; Laupretre, F. *Macromolecules* **2005**, *38*, 2786–2794.
- (26) Sanchis, M. J.; Diaz-Calleja, R.; Pelissou, O.; Gargallo, L.; Radic, D. *Polymer* **2004**, *45*, 1845–1855.
- (27) Tadano, K.; Tanaka, Y.; Shimizu, T.; Yano, S. *Macromolecules* **1999**, *32*, 1651–1660.
- (28) Zhang, Q.; Archer, L. A. *J. Phys. Chem. B* **2006**, *110*, 4924–4928.
- (29) Boyd, R. H.; Breitlin, S. *Macromolecules* **1974**, *7*, 855–862.
- (30) Koizumi, S.; Tadano, K.; Tanaka, Y.; Shimidzu, T.; Kutsumizu, S.; Yano, S. *Macromolecules* **1992**, *25*, 6563–6567.
- (31) Mohomed, K.; Gerasimov, T. G.; Moussy, F.; Harmon, J. P. *Polymer* **2005**, *46*, 3847–3855.
- (32) Daniel, V. V., *Dielectric Relaxation*; Academic Press: London and New York, 1967.
- (33) Horansky, R. D.; Clarke, L. I.; Price, J. C.; Khuong, T. A. V.; Jarowski, P. D.; Garcia-Garibay, M. A. *Phys. Rev. B* **2005**, *72*, 014302.